Pergamon

Int. J. Heat Mass Transfer. Vol. 40, No. 16, pp. 3883–3897, 1997

Printed in Great Britain
0017–9310/97 $17.00 + 0.00

PII: S0017-9310(97)00016-1

Nonisothermal extrusion flow of viscoplastic fluids with wall slip

ADENIYI LAWAL

Department of Chemical Engineering, King Fahd University of Petroleum & Minerals, Dhahran 31261, Saudi Arabia

and

DILHAN M. KALYON

Highly Filled Materials Institute, Chemistry and Chemical Engineering Department, Stevens Institute of Technology, Castle Point, Hoboken, NJ 07030, U.S.A.

(*Received* 1 *July* 1996 *and in final form* 9 *January* 1997)

Abstract—The extrusion flow of viscoplastic fluids in shallow channels can be modeled as that occurring between two infinitely long parallel plates, i.e. the generalized plane Couette flow. Commonly encountered viscoplastic fluids including concentrated suspensions exhibit apparent slip in extrusion processing. Various factors, including the roughness of the wall surface, affect wall slip behavior, and the highly viscous nature of the processed materials implies significant viscous dissipation effects. Here, we develop an analytical nonisothermal model of the extrusion of viscoplastic fluids subject to wall slip. The model accommodates different slip coefficients at the screw and barrel surfaces. Closed-form expressions for the velocity and temperature distributions, as well as the bulk temperature valid from the entrance to the exit of the extruder are presented. The conservation of energy equation is solved using the finite integral transform technique. The accuracy of the obtained solutions is established and the effects of various parameters examined. © 1997 Elsevier Science Ltd.

INTRODUCTION

The single screw and the fully intermeshing co-rotating twin screw extruders are perhaps two of the most commonly used continuous processors for highly viscous polymeric fluids. They rely on drag-induced flow and pressurization, whereby the fluid is conveyed and pressurized by the action of at least one moving surface. Consequently, the polymeric fluid is subject to varying deformation rates. Owing to the highly viscous nature of these materials, for a high deformation rate, the shearing of fluid layers generates a considerable amount of mechanical energy which is irreversibly dissipated as heat energy. The transverse variation of the deformation rate in the screw channel, as well as the dependence of the shear viscosity of the fluid on the deformation rate implies that this viscous energy dissipation can lead to significantly high local temperature rises to the extent that they can far exceed the bulk temperature rises.

Various mathematical models of differing degrees of complexity [1–5] have been proposed for the modeling of nonisothermal extrusion flow of polymeric fluids. As a first approximation, the geometry of the screw extruder is usually unwound in the channel direction. Fenner [6] has investigated various solution methods available for the flow and deformation occurring in the single screw extruder, and Zamodits and Pearson [7] presented screw characteristic curves for a rectangular channel for different values of the power-law index. Nonisothermal analyses have been performed by Colwell and Nicholls [8], and Griffith [9]. To properly account for curvature effect, a finite element method based formulation is required, but is too complicated for general adaptation and use [10]. Denson and Hwang [1] analyzed the flow in several actual geometries for a Newtonian fluid, using the finite element method. However, for shallow screws, the curvature effects can be neglected without incurring significant errors. For such screw geometries, the flow so obtained, i.e. the generalized plane Couette flow provides an excellent model description of the flow. Closed form analytical expressions can then be easily worked out for the velocity distribution and, hence, the functional dependence of the throughput rate on the pressure generated for various design parameters and operating conditions. For constant property fluids, the thermal problem can also be similarly handled.

All the foregoing nonisothermal studies which are based on the parallel-plate configuration were concerned with power-law fluids, but a large number of materials processed in screw extrusion are not adequately characterized by this rheological behavior. Of these various materials, the highly filled suspensions of polymeric composites, and energetics

NOMENCLATURE

$a_m(z^*)$	expansion coefficient defined by equation (16b)
Bi_0	Biot modulus at screw surface
Bi_1	Biot modulus at barrel surface
C_p	specific heat capacity
$c(y)$	inlet temperature distribution
$C(\xi)$	dimensionless inlet temperature distribution
dP/dz	pressure gradient
$f(\xi)$	viscous dissipation function defined by equation (13)
G	Griffith number
h_0	heat transfer coefficient at screw surface
h_1	heat transfer coefficient at barrel surface
H	channel depth
k	thermal conductivity
m	material parameter
n	parameter governing the sensitivity of fluid to deformation rate
$\mathbf{n}$	unit outward normal vector
N_m	normalization integral defined by equation (16c)
$Pé$	Péclet number
s	reciprocal of n
$\mathbf{t}$	unit tangent vector
T	temperature
T^*	reference temperature
$\mathbf{u}$	velocity vector of fluid
$\mathbf{u}_{solid}$	velocity vector of solid surface
u_z	velocity in the z-coordinate direction
u_z^*	dimensionless velocity in the z-coordinate direction
V_w	linear screw velocity
y	y-coordinate transverse direction
z	z-coordinate axial direction
z^*	dimensionless z-coordinate.

Greek symbols

α_1	dimensionless slip coefficient at the screw surface
α_2	dimensionless slip coefficient at the barrel surface
β	Navier's slip coefficient
β_b	slip coefficient at the screw surface
β_t	slip coefficient at the barrel surface
$\lvert\dot{\gamma}\rvert$	magnitude of the deformation rate
Λ	dimensionless pressure gradient defined by equation (3a)
ψ_m	eigenfunction of eigenproblem defined by equation (14a–c)
η	shear viscosity material function
κ_1	dimensionless ratio of slip coefficient to yield stress at the screw surface
κ_2	dimensionless ratio of slip coefficient to yield stress at the barrel surface
λ_m^2	eigenvalues of eigenproblem defined by equation (14a–c)
$\boldsymbol{\pi}$	total stress tensor
θ	dimensionless temperature defined by equation (11a)
θ_b	dimensionless bulk temperature defined by equation (25a)
$\overline{\theta}_m$	integral transform of θ
ρ	fluid density
τ_0	apparent yield stress
τ_{yz}	shearing stress
ω	dimensionless volume flow rate
Ω	transverse coordinate
ξ	dimensionless transverse coordinate defined by equation (3a).

deserve particular attention, as their rheological behavior presents special processing challenges. Not only do these materials exhibit viscoplasticity (i.e. below a critical value of the stress magnitude, they do not deform), which significantly affects their processability, but their flow and deformation is also further complicated by the concomitant occurrence of apparent wall slip at solid surfaces. Thus, a realistic model for the processing of these viscoplastic materials should incorporate the wall slip boundary condition at solid surfaces.

The occurrence of wall slip, i.e. a relative velocity between the fluid velocity at the wall and the wall velocity is well documented for a variety of fluids including gels and concentrated suspensions [11–13], polyethylenes [14–18]. The wall slip behavior of a concentrated suspension consisting of a 60% by volume glass spheres in an acrylonitrile terminated polybutadiene matrix is demonstrated in Fig. 1. The suspension sample undergoes steady torsional flow in between two parallel disks; the top one is rotating, while the bottom one is stationary. Before the onset of deformation, a straight line marker is placed at the free surface of the suspension and the edges of the two disks as shown in Fig. 1. Upon deformation, discontinuities appear at both suspension/wall interfaces suggesting apparent wall slip. In Fig. 2, the viscoplastic suspension has an affinity for wall slip at the bottom plate and exhibits a no slip condition at the top plate. This behavior is effected by the roughness intentionally machined onto the surface of the top disk. This experiment demonstrates that techniques involving selections of surface roughness and material of construction provide the capability to engineer the wall slip behavior of viscoplastic fluids.

The wall slip vs the wall shear stress behavior of

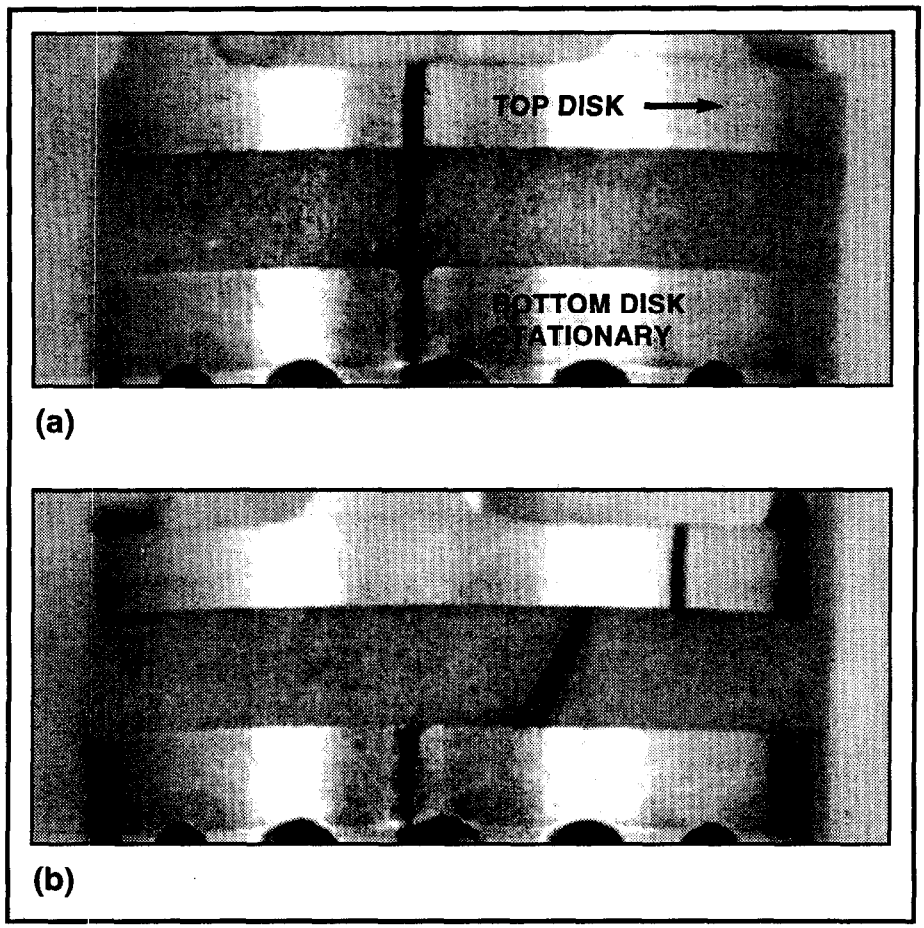

Fig. 1. Wall slip behaviour of a concentrated suspension containing 60% solid glass spheres in an acrylonitrile terminated polybutadiene, PBAN, matrix at 25°C in torsional flow. Both surfaces are smooth surfaces.

fluids which exhibit apparent slip can be characterized by employing viscometric flows [19, 12]. The data on the wall slip velocity u_s vs wall shear stress τ_w can be fitted by [19, 12]:

$$u_s = \beta\tau_w$$

where β is a material constant, i.e. Navier's wall slip coefficient, and can be temperature dependent. It is this capability to characterize an interfacial constitutive equation for various fluids which renders the analysis contained in this article especially relevant.

The objectives of the present study include the presentation of analytical and exact solutions for the velocity and temperature distributions for the problem of nonisothermal extrusion of viscoplastic fluids subject to Navier wall slip condition at the barrel and screw surfaces. The flow and heat transfer in the screw extruder is modeled as that occurring between two infinite parallel plates representing the screw and barrel surfaces. The thermal boundary condition is given by an arbitrary heat transfer coefficient from which special cases are obtainable. The problem of solving the equation of conservation of energy is transformed to that of solving an eigenvalue problem using the finite integral transform technique [20, 21]. As many eigenvalues and eigenfunctions as required are determined using a very efficient and accurate method, the sign-count method [22].

ANALYSIS

Problem description

The steady nonisothermal flow of a viscoplastic fluid in the single screw extruder is modeled here as that occurring in a channel formed by two parallel plates in relative motion with the gap between the plates much smaller than the width of the channel. The inertia effect is usually negligible because of the highly viscous nature of the viscoplastic materials used in extrusion and the low Reynolds number of the resulting flow. In addition, viscoplastic liquids generally have low thermal conductivity and moderately high value of heat capacity, and hence exhibit high Prandtl numbers. In essence, the flow field will require a very short distance to attain a fully developed condition in comparison with the temperature field. Therefore, the flow can be accurately modeled as hydrodynamically developed but thermally developing at

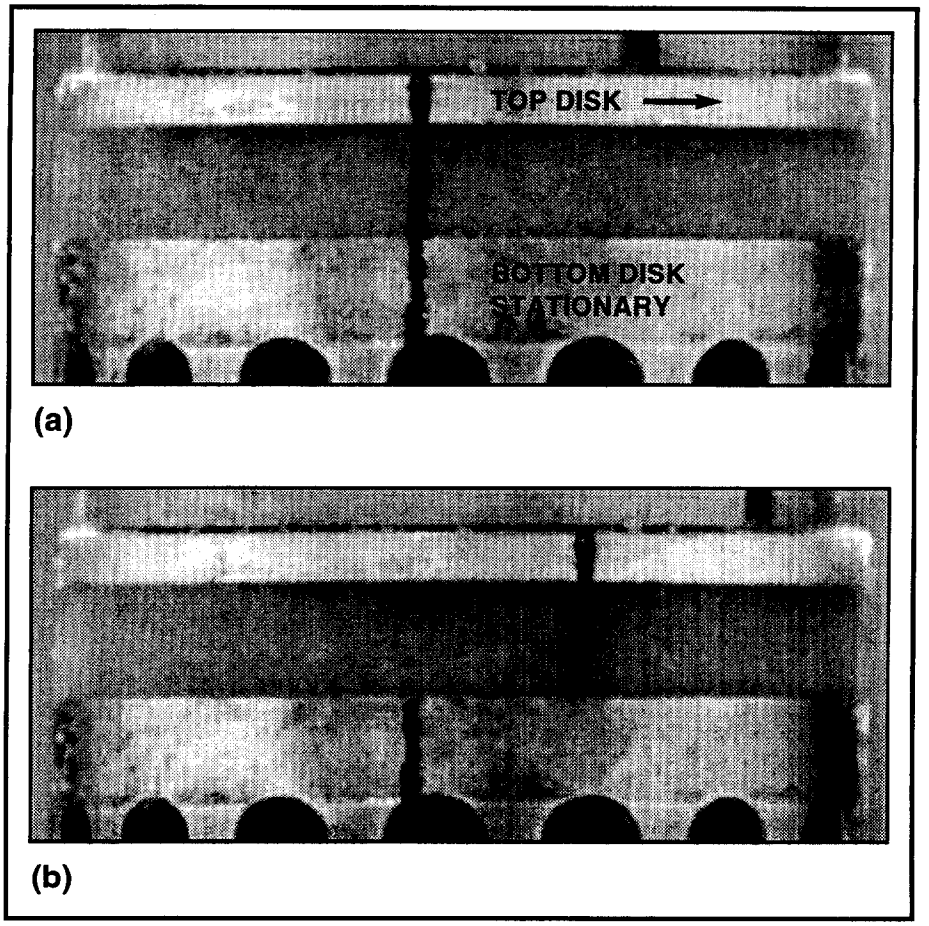

Fig. 2. Torsional flow of a concentrated suspension consisting 60% by volume glass spheres in PBAN matrix affected by the presence of a roughened surface at the top and smooth surface at the bottom.

the entrance to the extruder. Related to this is the high Péclet number ($Pé > 10^3$) associated with polymer processing operations which enables the neglect of heat conduction in the downchannel direction except for very low volume flow rates and the region very close to the entrance.

The fluid enters the screw channel of depth H (Fig. 3) with a known temperature distribution and flows in the axial direction with the viscous heat generating local temperature variations in both y- and z-directions. On both the screw surface and the barrel, the heat flux will be given by a heat transfer coefficient thus permitting various thermal boundary conditions, including as limiting cases, the isothermal and the adiabatic conditions. Variations of the physical properties of the fluid (such as the shear viscosity, density and heat capacity) due to temperature are assumed negligible, hence the thermal and momentum problems are decoupled.

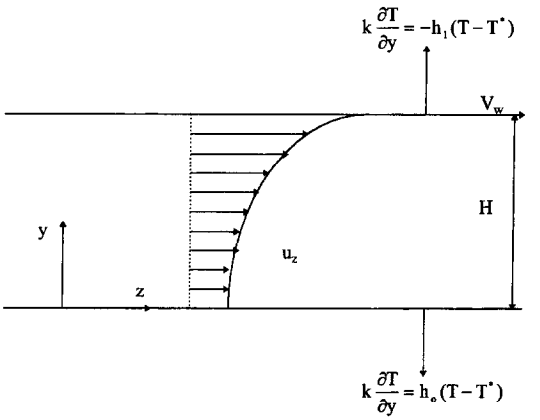

Fig. 3. Schematic of the considered model of extrusion flow with the fluid entering at $z = 0$ with specified inlet temperature $c(y)$ and fully developed velocity $u_z(y)$.

Velocity field

The equation of conservation of momentum for this one-dimensional flow is given by:

$$\frac{-d\tau_{yz}}{dy} = \frac{dP}{dz} \tag{1}$$

where y is the transverse coordinate, P is the pressure and τ_{yz} is the shearing stress. In the screw extruder, dP/dz is positive for dynamic viscous pressurization. To obtain a solution to equation (1), a constitutive model need be specified. Here, the fluid is assumed to

be a purely viscous fluid that can be characterized rheologically by the Herschel–Bulkley model:

$$\tau_{yz} = -m\left|\frac{du_z}{dy}\right|^{n-1}\frac{du_z}{dy} \pm \tau_0 \quad |\tau_{yz}| \geqslant \tau_0 \tag{2a}$$

$$\frac{du_z}{dy} = 0 \quad |\tau_{yz}| \leqslant \tau_0. \tag{2b}$$

Here, m and n are material parameters and τ_0 is the yield stress, i.e. a critical value of the stress magnitude below which viscoplastic materials do not deform. The minus sign is to be used when $\tau_{yz} < 0$. At stress magnitudes $|\tau_{yz}|$ which are les than the yield stress, only the rigid body motion, i.e. plug flow is possible.

Defining the following dimensionless variables:

$$u_z^* = \frac{u_z}{V_w}; \quad \xi = \frac{y}{H}; \quad \Lambda = \left(\frac{H^{n+1}}{mV_w^n}\right)\frac{dP}{dz}. \tag{3a}$$

Equation (1) becomes:

$$\frac{d}{d\xi}\left(\left|\frac{du_z^*}{d\xi}\right|^{n-1}\frac{du_z^*}{d\xi}\right) = \Lambda. \tag{3b}$$

Equation (3b) is applicable only in the deformation region and is replaced by the rigid body translation requirement, equation (2b), in the plug region whenever it exists. The boundary conditions to equation (3b) are provided by the Navier's slip at the wall condition which is of the form [23]:

$$\mathbf{t}\cdot(\mathbf{u}-\mathbf{u}_{solid}) = \beta\mathbf{n}\mathbf{t}:\boldsymbol{\pi} \tag{4}$$

where $\mathbf{t}$ is the unit tangent vector to the surface, $\mathbf{n}$ the unit outward normal and β is the slip parameter. The limits for $\beta = \infty$ and $\beta = 0$ give perfect slip and no slip conditions, respectively. $\mathbf{u}$ and $\mathbf{u}_{solid}$ are the velocity vectors of the fluid and the solid surface, respectively, and $\boldsymbol{\pi}$ is the total stress tensor.

Returning to equation (3b), three distinct cases are possible, Fig. 4, depending on the values of the parameters of the problem. The solutions to these cases have been worked out by Lawal and Kalyon [5] and are as follows:

Case A: *no plug region*. This case obtains when

$$\frac{\Lambda^s}{(s+1)} \leqslant 1-\kappa_1-\kappa_2+\alpha_2 \tag{5a}$$

and the velocity distribution is:

$$u_z^* = \frac{\Lambda^s}{(s+1)}(\xi-\lambda_2)^{s+1} - \frac{\Lambda^s}{(s+1)}(-\lambda_2)^{s+1} + \kappa_1+\alpha_1\lambda_2 \quad 0 \leqslant \xi \leqslant 1. \tag{5b}$$

The parameter λ_2 is obtained from

$$\frac{\Lambda^s}{(s+1)}(1-\lambda_2)^{s+1} - \frac{\Lambda^s}{(s+1)}(-\lambda_2)^{s+1} + \kappa_1+\alpha_1\lambda_2+\kappa_2+\alpha_2(\lambda_2-1)-1 = 0. \tag{5c}$$

In these equations and all the ones to be presented subsequently, we have $s = 1/n$, $\kappa_1 = \beta_b\tau_0/V_w$, $\alpha_1 = (\beta_b H/V_w)(-dP/dz)$, $\kappa_2 = \beta_t\tau_0/V_w$ and $\alpha_2 = (\beta_t H/V_w)(-dP/dz)$. β_b and β_t are the slip parameters at the bottom and top surfaces, respectively.

Case B: *plug attached to the bottom surface.*

$$u_z^* = 1 - \frac{\Lambda^s}{(s+1)}(1-\lambda_2)^{s+1} - \kappa_2 - \alpha_2(\lambda_2-1) \quad 0 \leqslant \xi \leqslant \lambda_2 \tag{6a}$$

$$u_z^* = \frac{\Lambda^s}{(s+1)}(\xi-\lambda_2)^{s+1} - \frac{\Lambda^s}{(s+1)}(1-\lambda_2)^{s+1} - \kappa_2 - \alpha_2(\lambda_2-1)+1 \quad \lambda_2 \leqslant \xi \leqslant 1. \tag{6b}$$

λ_2 is given by the equation:

$$\frac{\Lambda^s}{(s+1)}(1-\lambda_2)^{s+1} + \kappa_1 + \alpha_1\lambda_2 + \kappa_2 + \alpha_2(\lambda_2-1) - 1 = 0. \tag{6c}$$

The following processing conditions must be met for Case B to occur:

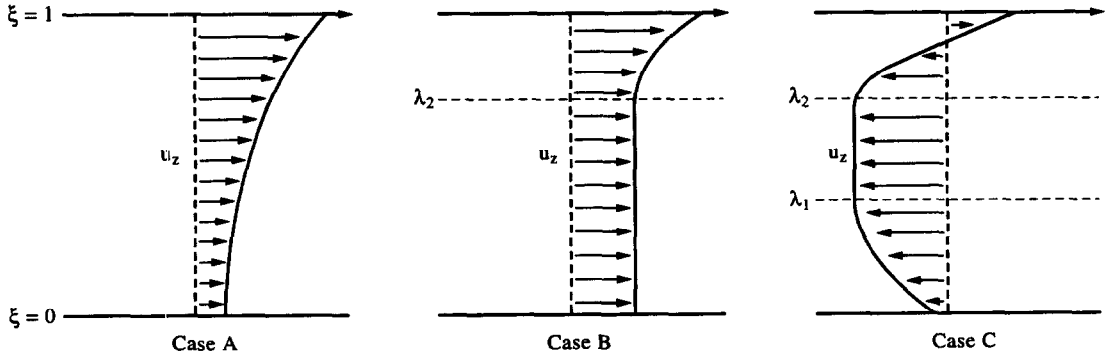

Fig. 4. Schematic representations of the velocity profiles for the three cases for positive dynamic pressurization.

$$\frac{\Lambda^s}{(s+1)} \geqslant 1-\kappa_1-\kappa_2+\alpha_2 \tag{7a}$$

$$\lambda_2-\lambda_1 = \left(\frac{2\tau_0}{H\,\mathrm{d}P/\mathrm{d}z}\right) \geqslant 1 \tag{7b}$$

or

$$\lambda_2-\lambda_1 \geqslant \lambda^* \tag{7c}$$

where λ^* is determined from:

$$\frac{\Lambda^s}{(s+1)}(1-\lambda^*)^{s+1}+\kappa_1+\alpha_1\lambda^*+\kappa_2 +\alpha_2(\lambda^*-1)-1=0. \tag{7d}$$

Case C: floating plug region.

$$u_z^* = \frac{\Lambda^s}{(s+1)}(\lambda_1-\xi)^{s+1} - \frac{\Lambda^s}{(s+1)}\lambda_1^{s+1}+\kappa_1+\alpha_1\lambda_2 \quad 0 \leqslant \xi \leqslant \lambda_1 \tag{8a}$$

$$u_z^* = 1-\frac{\Lambda^s}{(s+1)}(1-\lambda_2)^{s+1} -\kappa_2+\alpha_2(\lambda_2-1) \quad \lambda_1 \leqslant \xi \leqslant \lambda_2 \tag{8b}$$

$$u_z^* = \frac{\Lambda^s}{(s+1)}(\xi-\lambda_2)^{s+1} - \frac{\Lambda^s}{(s+1)}(1-\lambda_2)^{s+1}-\kappa_2-\alpha_2(\lambda_2-1)+1 \quad \lambda_2 \leqslant \xi \leqslant 1. \tag{8c}$$

The equation for λ_2 is provided by:

$$1-\frac{\Lambda^s}{(s+1)}(1-\lambda_2)^{s+1} -\kappa_1-\alpha_1\lambda_2-\kappa_2-\alpha_2(\lambda_2-1) + \frac{\Lambda^s}{(s+1)}\left(\lambda_2-\frac{2\tau_0}{H\dfrac{\mathrm{d}P}{\mathrm{d}z}}\right)^{s+1}=0 \tag{8d}$$

and λ_1, subsequently, obtained from:

$$\lambda_2-\lambda_1 = \frac{2\tau_0}{H\dfrac{\mathrm{d}P}{\mathrm{d}z}}. \tag{8e}$$

The processing conditions that will give rise to Case C are given by equation (7a) and

$$\lambda_2-\lambda_1 \leqslant \lambda^* \tag{9}$$

with λ^* again determined from equation (7d).

Temperature field

With the assumptions given earlier, the thermal problem is described by the equation:

$$\rho C_p u_z\frac{\partial T}{\partial z} = k\frac{\partial^2 T}{\partial y^2}+\eta|\dot\gamma|^2 \tag{10a}$$

subject to the following conditions:

$$T = c(y); \quad z=0,\ 0 \leqslant y \leqslant H \tag{10b}$$

$$k\frac{\partial T}{\partial y} = h_0(T-T^*); \quad z>0,\ y=0 \tag{10c}$$

$$k\frac{\partial T}{\partial y} = -h_1(T-T^*); \quad z>0,\ y=H. \tag{10d}$$

In equation (10), η is the shear viscosity which is obtainable from equation (2a), $|\dot\gamma|$ is the magnitude of the rate-of-deformation tensor, $c(y)$ is the inlet temperature distribution, and T^* is a reference temperature. To render the equations dimensionless, we define the following variables:

$$\theta = \frac{T-T^*}{\Delta T} \tag{11a}$$

$$z^* = z/HP\acute{e} \tag{11b}$$

$$\tau_0^* = \tau_0/m(V_w/H)^n \tag{11c}$$

where $P\acute{e} = \rho C_p V_w H/k$ is the Péclet number and ΔT is a reference temperature difference. On substituting for η and $|\dot\gamma|$ in terms of the velocity gradient, and introducing the dimensionless variables, equation (10) becomes:

$$u_z^*\frac{\partial\theta}{\partial z^*} = \frac{\partial^2\theta}{\partial\xi^2}+Gf(\xi) \tag{12a}$$

$$\theta = C(\xi); \quad z^*=0,\ 0 \leqslant \xi \leqslant 1 \tag{12b}$$

$$\frac{\partial\theta}{\partial\xi} = +Bi_0\theta; \quad z^*>0,\ \xi=0 \tag{12c}$$

$$\frac{\partial\theta}{\partial\xi} = -Bi_1\theta; \quad z^*>0,\ \xi=1 \tag{12d}$$

where $G = m(V_w/H)^{n-1}\,V_w^2/k\,\Delta T$ is the Griffith number (generally referred to as the Brinkmann number for the Newtonian fluid), $Bi_0 = h_0H/k$, $Bi_1 = h_1H/k$ are Biot moduli and $f(\xi)$, the viscous dissipation function is given by:

$$f(\xi) = \left|\frac{\mathrm{d}u_z^*}{\mathrm{d}\xi}\right|^{n+1}+\tau_0^*\left|\frac{\mathrm{d}u_z^*}{\mathrm{d}\xi}\right|. \tag{13}$$

The velocity gradient can be evaluated from the appropriate equation of any of those earlier presented.

To solve equation (12a–d), we apply the finite integral transform technique. The appropriate eigenvalue problem for equation (12a–d) is taken as:

$$\nabla\cdot\nabla\psi_m+\lambda_m^2u_z^*\psi_m = 0 \tag{14a}$$

subject to the following boundary conditions

$$\left.\frac{\mathrm{d}\psi_m(\lambda_m,\xi)}{\mathrm{d}\xi}\right|_{\xi=0} = +Bi_0\psi_m \tag{14b}$$

$$\left.\frac{d\psi_m(\lambda_m,\xi)}{d\xi}\right|_{\xi=1} = -Bi_1\psi_m \tag{14c}$$

with ψ_m and λ_m^2 being the eigenfunctions and the eigenvalues, respectively. Using equation (14a–c), the eigenfunctions ψ_m can be shown to be orthogonal with respect to the weighting function u_z^* such that:

$$\iint u_z^*\psi_m(\xi)\psi_n(\xi)\,d\xi\,d\Omega = 0 \quad \text{for } m \neq n \tag{15}$$

where the integration is over the cross-sectional area of the channel and there is no dependency on the transverse Ω coordinate. The temperature θ can then be expanded in terms of the eigenfunctions $\psi_m(\xi)$ in the form:

$$\theta(\xi,z^*) = \sum_{m=1}^{\infty} a_m(z^*)\psi_m(\xi) \tag{16a}$$

and using the orthogonality condition, equation (15), the expansion coefficients $a_m(z^*)$ are determined to be:

$$a_m(z^*) = \frac{1}{N_m}\int\int u_z^*\psi_m\theta\,d\xi\,d\Omega \tag{16b}$$

where

$$N_m = \iint u_z^*\psi_m^2\,d\xi\,d\Omega. \tag{16c}$$

Equation (16a–c) can now be written as the finite integral transform and the inversion of the function $\theta(\xi,z^*)$ in the forms:

$$\overline{\theta_m}(z^*) = \iint u_z^*K_m\theta\,d\xi\,d\Omega \tag{17a}$$

$$\theta(\xi,z^*) = \sum_{m=1}^{\infty} K_m(\xi)\overline{\theta_m}(z^*) \tag{17b}$$

where $K_m(\xi)$ is the normalized eigenfunction

$$K_m(\xi) = \frac{\psi_m(\xi)}{\sqrt{N_m}}. \tag{17c}$$

The integral transform and the inversion will now be employed in the solution of equation (12a–d). Equation (12a) is first multiplied by K_m and then integrated over the cross-sectional area of the channel to obtain:

$$\iint u_z^*\frac{\partial\theta}{\partial z^*}K_m\,d\xi\,d\Omega = \iint(\nabla\cdot\nabla\theta)K_m\,d\xi\,d\Omega + \iint Gf(\xi)K_m\,d\xi\,d\Omega. \tag{18}$$

Upon the application of Green's theorem, and the assumption of non-dependency of the integrand on the transverse coordinate Ω, the first term on the right hand side of equation (18) becomes:

$$\iint(\nabla\cdot\nabla\theta)K_m\,d\xi\,d\Omega = \iint\theta(\nabla\cdot\nabla K_m)\,d\xi\,d\Omega + \Omega_s K_m\left.\frac{\partial\theta}{\partial\xi}\right|_0^1 - \Omega_s\theta\left.\frac{\partial K_m}{\partial\xi}\right|_0^1. \tag{19}$$

We can utilize equations (12c–d) and (14b–c) to simplify equation (18), thus:

$$\iint u_z^*\frac{\partial\theta}{\partial z^*}K_m\,d\xi\,d\Omega = \iint\theta(\nabla\cdot\nabla K_m)\,d\xi\,d\Omega + \iint Gf(\xi)K_m\,d\xi\,d\Omega. \tag{20}$$

Upon the substitution for the first term on the right hand side using equation (14a), equation (20) reduces to:

$$\frac{d}{dz^*}\iint u_z^*\theta K_m\,d\xi\,d\Omega + \lambda_m^2\iint u_z^*\theta K_m\,d\xi\,d\Omega = \iint Gf(\xi)K_m\,d\xi\,d\Omega \tag{21a}$$

or

$$\frac{d\overline{\theta_m}}{dz^*} + \lambda_m^2\overline{\theta_m} = \iint Gf(\xi)K_m\,d\xi\,d\Omega. \tag{21b}$$

Equation (21b) is a first-order ordinary differential equation and the appropriate initial condition is provided by equation (12b):

$$\overline{\theta}(0) = \Omega_s\int_0^1 u_z^*K_mC(\xi)\,d\xi. \tag{22}$$

The solution to equation (21) subject to equation (22) is:

$$\overline{\theta}(z^*) = \frac{(\iint Gf(\xi)K_m\,d\xi\,d\Omega)(1-\exp(-\lambda_m^2z^*))}{\lambda_m^2} + \left[\Omega_s\int_0^1 u_z^*K_mC(\xi)\,d\xi\right]\exp(-\lambda_m^2z^*). \tag{23}$$

Finally, the inversion of the transform provides the solution for θ in the form:

$$\theta = \sum_{m=1}^{\infty}\frac{\psi_m}{\int_0^1 u_z^*\psi_m^2\,d\xi} \times\left[\frac{\left(\int_0^1 Gf(\xi)\psi_m\,d\xi\right)(1-\exp(-\lambda_m^2z^*))}{\lambda_m^2} + \left(\int_0^1 u_z^*\psi_mC(\xi)\,d\xi\right)\exp(-\lambda_m^2z^*)\right]. \tag{24}$$

The dimensionless bulk temperature θ_b is defined as

$$\theta_b = \frac{\int_0^1\theta u_z^*d\xi}{\omega} \tag{25a}$$

Table 1. Boundary conditions for the temperature problem

Wall condition	Reference quantities and dimensionless parameters T^*	ΔT	$C(\xi)$	Bi_0	Bi_1
Isothermal barrel adiabatic screw	T_b	T_0-T_b	1	0	∞
Isothermal barrel and screw	T_b	T_0-T_b	1	∞	∞
Adiabatic screw and barrel	T_0	T_0	0	0	0
Arbitrary heat transfer coefficient	T_0	T_0	0	Bi_0	Bi_1

where ω, the dimensionless volume flow rate is given by

$$\omega = \int_0^1 u_z^* \mathrm{d}\xi \tag{25b}$$

and is obtainable in closed form by integrating the appropriate velocity profile. Upon the substitution for θ and u_z^* and the evaluation of the integrals, we have:

$$\theta_b = \frac{1}{\omega}\sum_{m=1}^{\infty}\frac{\int_0^1 u_z^*\psi_m \mathrm{d}\xi}{\int_0^1 u_z^*\psi_m^2 \mathrm{d}\xi}\left[\frac{\int_0^1 Gf(\xi)\psi_m \mathrm{d}\xi}{\lambda_m^2}\right.$$
$$\times(1-\exp(-\lambda_m^2 z^*))+\left(\int_0^1 u_z^*\psi_m C(\xi)\mathrm{d}\xi\right)$$
$$\left.\times\exp(-\lambda_m^2 z^*)\right]. \tag{25c}$$

The evaluation of the temperature field from equations (24) and (25) requires the knowledge of the eigenvalues as well as the eigenfunctions of the eigenvalue problem described by equation (14a–c). In order to overcome the difficulties that generally arise in the determination of the eigenvalues and eigenfunctions of this class of problems, we have implemented an accurate and efficient method, the sign-count method, the details of which are described elsewhere [22]. The procedure enables the exact analytical determination of as many eigenvalues as required without resorting to numerical techniques such as finite differencing [24], or approximate analytical solution methods [25].

The general solutions developed above for the temperature field include several interesting cases some of which are indicated in Table 1. In all these cases, the fluid is assumed to enter the screw channel with a uniform temperature T_0. With the screw and barrel surfaces adiabatic, the first eigenvalue λ_1^2 is zero, consequently the first term on the right-hand side of each of equations (24) and (25) is evaluated using L'Hopital's rule.

RESULTS AND DISCUSSION

Given the rheological parameters, as well as the processing and operating conditions, equations (5a), (7a–c) and (9) can be used in selecting the appropriate cases among the three possible velocity profiles. This necessitates the solution of the corresponding nonlinear equations for the values of the extremum locations λ_1, λ_2 and λ^*, a task that was accomplished by using the standard Newton–Raphson's technique. The general relative tolerance was set to 10^{-6} in obtaining the velocity profiles. The eigenvalues and eigenfunctions of equation (14a–c) which are needed in the determination of the temperature distributions were obtained with the same general relative tolerance. The number of terms retained in the series expansion solutions (equations (24) and (25)) was varied from 20 to 80, and the deviations in the calculated local and bulk temperatures were found to be insignificant beyond 50 terms for the range of parameters considered in this study, and for all values of the axial coordinate z^*. Hence, all the results to be presented, subsequently, were obtained with 50 terms.

Comparison of analytical solutions with limiting cases and experimental data

The analytical solutions for the velocity distributions were verified by comparing our results with well-known results available in the literature. Amongst the results selected for comparison were those of Denson and Hwang [1] who obtained a numerical-solution based empirical screw characteristic equation for a twin-screw extruder. As indicated in Fig. 5(a), excellent agreement was found between our computed mass flow rate and that predicted by the equation of Denson and Hwang [1], and for a wide range of pressure gradient values, the differences between the results are imperceptible. The outcome was the same for other non-isothermal results utilized in the verification of the accuracy of the analytical velocity profiles.

The analytical solutions for the temperature distributions were compared with experimental temperature measurements obtained from the work of Esseghir and Sernas [26] on temperature distribution in a single screw extruder. The inlet temperature of

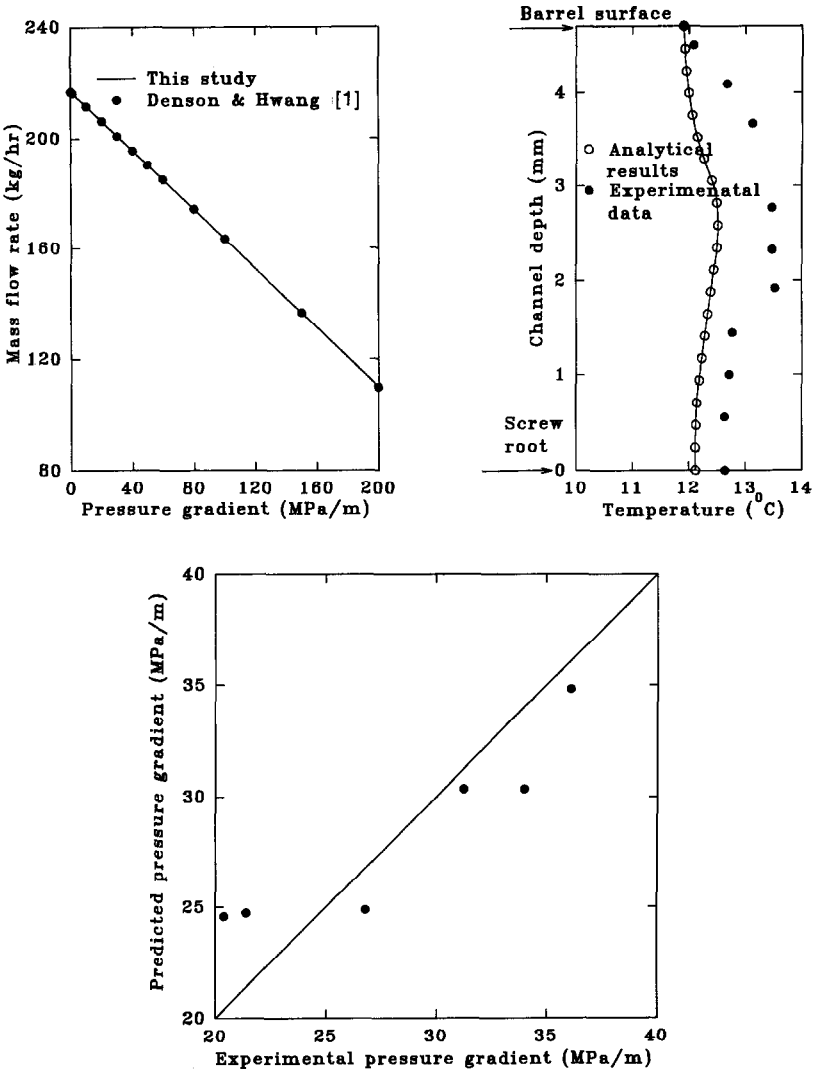

Fig. 5. (a) Comparison of model predictions of the present study with the numerical results of Denson and Hwang [1]; (b) comparison of numerical results of temperature distribution with experimental temperature distribution of Esseghir and Sernas [26]; (c) comparison of numerical results of pressure gradient with experimental pressure gradient measurements of Yaras [27].

the fluid to the non-isothermal section of the extruder was 22°C while the solid–fluid interface temperature at the barrel was kept at 11.9°C. Experimental temperature measurements confirmed an adiabatic thermal boundary condition at the screw root. Figure 5(b) shows the comparison between the predicted and experimental temperature distributions. The agreement is good and the differences can be accounted for by experimental error, and partly by the neglect of the curvature effects in the analysis which would have given rise to higher velocity gradients near the solid–fluid interfaces and, hence, higher viscous dissipation effects. The analytical solutions were also compared with experimental pressure gradient measurements obtained from the work of Yaras [27] on twin-screw extrusion of a highly concentrated suspension which exhibits viscoplasticity and apparent wall slip and has an activation energy close to zero (Fig. 5c). The differences between the results are again within the experimental error range, thus emphasizing that wall slip behavior (if present) must be properly accounted for and the rheological behavior carefully characterized if modeling is to predict reliable results.

Case studies

Having established the accuracy of the analytical solutions, we can next examine the effects of various parameters on the velocity and temperature profiles using a realistic set of parameters and operating conditions. However, due to space constraints, it is not possible to present comprehensive results which cover all the possible parameters and thermal boundary conditions, hence we will illustrate the solution with a small number of case studies. The values used are as indicated in Table 2 and the parametric variation indicated in the figures. The material parameters are

Table 2. The geometry, operating conditions, and material parameters used in the case studies

Material parameters
Herschel–Bulkley fluid
Shear-rate sensitivity parameter $n = 0.43$
$m = 6888$ Pa · s$^{0.43}$
$\tau_0 = 20$ Pa
Navier's wall slip coefficient $= 9.6 \times 10^{-8}$ m Pa^{-1} · s^{-1}
Density $= 1050.6$ kg m^{-3}
Specific heat capacity $= 1078$ J kg^{-1} K^{-1}
Thermal conductivity $= 0.206$ W (mK)$^{-1}$

Channel dimensions
Channel depth $= 1.15 \times 10^{-2}$ m
Channel width $= 2.54 \times 10^{-2}$ m

Operating conditions
Linear screw velocity $= 0.393$ m s^{-1}
Volume flow rate $= 9.52 \times 10^{-2}$ m^3 h^{-1}
Entrance temperature $= 298$ K

those of a highly filled polymer suspension with a matrix of Dow Corning poly (dimethylsiloxane) 200 and filled at 60% level with borosilicate hollow glass spheres [27]. The suspension was characterized by employing Instron Capillary Rheometer [27], steady torsional rheometrics system IV [28], and on-line rectangular slit rheometer [29]. The dependence of the wall shear stress vs shear rate data on the capillary diameter at constant length/diameter ratio indicated the presence of wall slip, and the slip coefficient was determined by methods already detailed elsewhere [19, 12]. The yield stress value of the suspension τ_0, was determined separately using small amplitude oscillatory shear experiments [28]. The rheological data were fitted with the Herschel–Bulkley constitutive model. The other properties were obtained by conventional methods.

(*a*) *Effect of the slip coefficient* β. For the conditions of Table 2, the effect of wall slip on the pressurization capability of the extruder when both the screw and barrel surfaces have the same slip coefficient β, is shown in Fig. 6(a). As the wall slip coefficient β increases, the mass flow rate decreases for the same pressurization capability. For every β value, above a certain pressure gradient, it is not possible to achieve a positive mass flow rate. Wall slip reduces the velocity gradients, thereby reducing the pressure gradient. If wall slip is ignored, i.e. the Navier's slip coefficient β is taken as zero, the velocity of the fluid at any solid surface takes on the same value as that of the surface. However, on incorporation of wall slip as seen from Fig. 6(b), the fluid velocity at either the screw surface or the barrel wall attains a non-zero value. At the screw root, as the slip coefficient increases, so does the fluid velocity. Since the same mass flow rate is imposed, in order to satisfy the mass conservation constraint, we would expect that the increase in fluid velocity in the screw root region will be compensated for by a reduction in the fluid velocity as the barrel surface is approached. This is clearly observable in Fig. 6(b) where at the barrel surface, the fluid's velocity decreases as the slip coefficient β increases. The velocity gradient at the two solid surfaces exhibits the same behavior, i.e. increasing with β at the screw root but decreasing at the barrel surface.

Figure 6(c) presents corresponding dimensionless transverse temperature profiles for different values of β at a selected axial location, $z^* = 10^{-2}$ for the isothermal barrel and adiabatic screw, with the entrance temperature different from the barrel temperature. For each β value, the velocity gradient increases from the screw surface to the barrel surface and, thus, the viscous dissipation effect. The dimensionless temperature rise, therefore, increases from the screw surface (Fig. 6(c)) to some point in the region near the barrel surface where it attains a maximum value and is, subsequently, forced to reduce in order to meet the barrel wall temperature constraint. The fluid is essentially heating the barrel due to significant viscous dissipation effects. At any transverse location ξ, the dimensionless temperature rise decreases as the slip coefficient β increases. In the region close to the barrel, viscous dissipation dominates, and since increase in β results in decreased velocity gradient in this region (Fig. 6(b)), the dimensionless temperature rise decreases as β increases. In the screw root region, axial convection seems to be the dominant heat transfer mechanism as opposed to viscous dissipation. Even though the velocity gradient here decreases as β increases, the increased axial convection effect gives rise to a reduction in the dimensionless temperature rise.

If there is an effective transverse recirculatory flow in an extruder, a thermal boundary condition that may be obtained is that of isothermal barrel and screw surfaces with both at the same temperature, but different from the inlet fluid temperature. That such a condition is indeed attainable has been confirmed by experiment [30]. As indicated in Fig. 6(d), an increase in β produces a reduction in temperature and the maximum temperature rise obtainable is not significantly different from the adiabatic screw condition, regardless of the value of β. However, the cross-sectional average temperature rise is reduced except for very high value of β.

(*b*) *Effect of the ratio* $\beta_t/\beta_b(\varphi)$. The mass flow rate vs the pressurization rate behavior of the viscoplastic fluid under the conditions of Table 2, is shown in Fig. 7(a). The results are presented as a function of the slip coefficient at the top barrel surface β_t, over the slip coefficient at the bottom screw surface, β_b i.e. $\varphi = \beta_t/\beta_b$. The highest mass flow rate at any pressurization rate is obtained, when there is a no-slip condition at the barrel surface with a finite slip velocity at the screw surface, i.e. $\varphi = 0$. As the wall slip coefficient at the barrel surface increases, the production rate decreases for the same pressurization rate. These results can be employed in achieving optimum production rates by proper engineering of the

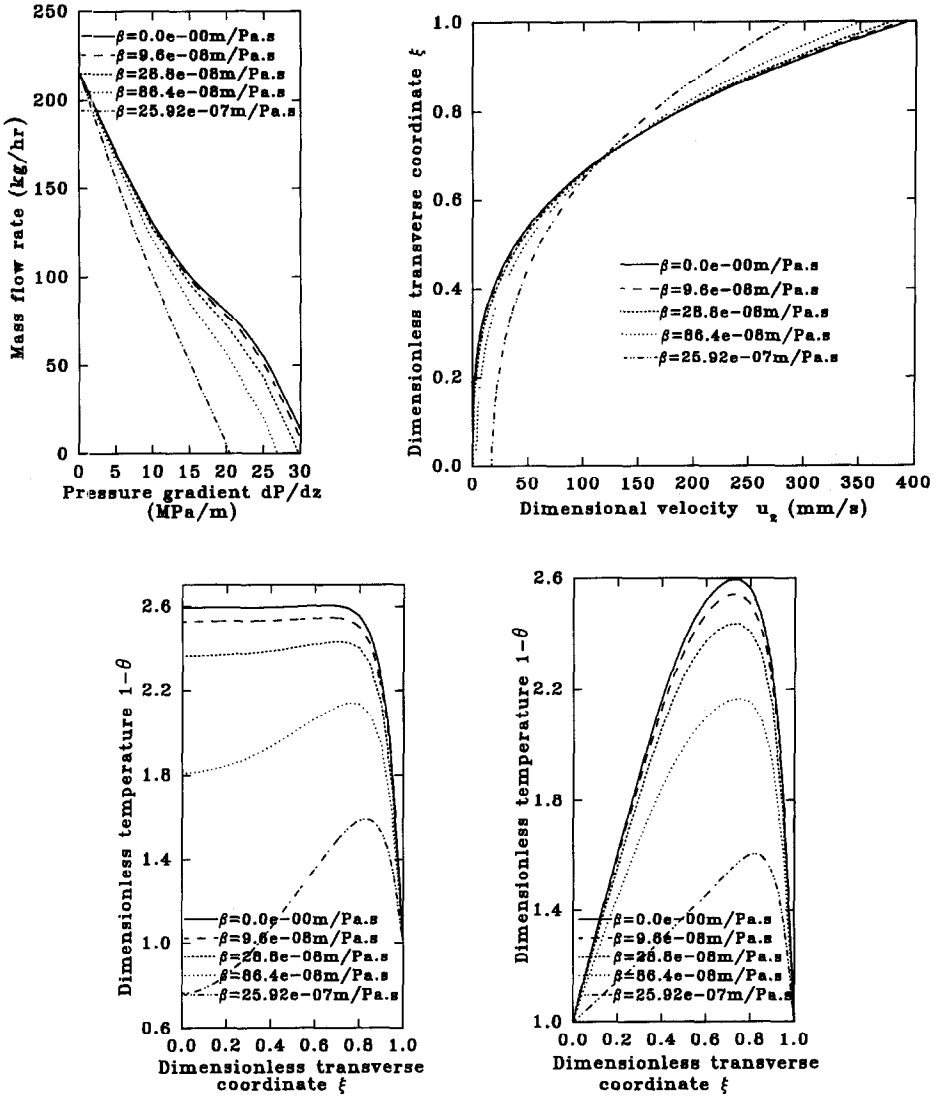

Fig. 6. (a) Mass flow rate vs pressure gradient relationship for an extruder for varying slip coefficient β with the screw and barrel having the same slip coefficient; (b) dimensional transverse velocity profiles in an extruder channel for varying slip coefficient β; (c) dimensionless transverse temperature profiles in an extruder channel with adiabatic screw root and isothermal barrel for varying slip coefficient β; (d) dimensionless transverse temperature profiles in an extruder channel with isothermal screw and barrel for varying slip coefficient β.

surfaces of the barrel and the screw in an extrusion process.

The effect of the ratio φ on the velocity profiles is depicted in Fig. 7(b). At the screw surface, the ratio φ does not seem to affect significantly the fluid velocity whereas at the barrel surface, the fluid velocity decreases as φ increases. However, the requirement of mass conservation results in a cross-over of the velocity profile from the screw root to the barrel surface. Correspondingly, the velocity gradient decreases at the barrel surface, and increases at the screw surface. The effect of φ on the temperature profiles is qualitatively similar to that of β, except that for the adiabatic screw condition, and for the chosen conditions of Table 2, the dimensionless temperature is never less than the barrel temperature.

(*c*) *Effect of yield stress* τ_0. The effect of the yield stress on the mass flow rate achievable given the desired pressurization rate or vice-versa is shown in Fig. 8(a). At low values of the pressurization rate, the yield stress exerts no significant influence on the mass flow rate. At higher pressurization rate, i.e. greater than 20 MPa m^{-1}, as the yield stress increases, the mass flow rate increases at constant pressurization (or conversely, pressurization rate increases at constant mass flow rate). This is related to the increased shear viscosity of the fluid as the yield stress increases. The corresponding velocity profiles are shown in Fig. 8(b), with the blown-up view of the profiles in the screw root region presented in Fig. 8(c). In the screw root region, the fluid's velocity increases as the yield stress increases while the velocity gradient decreases. The

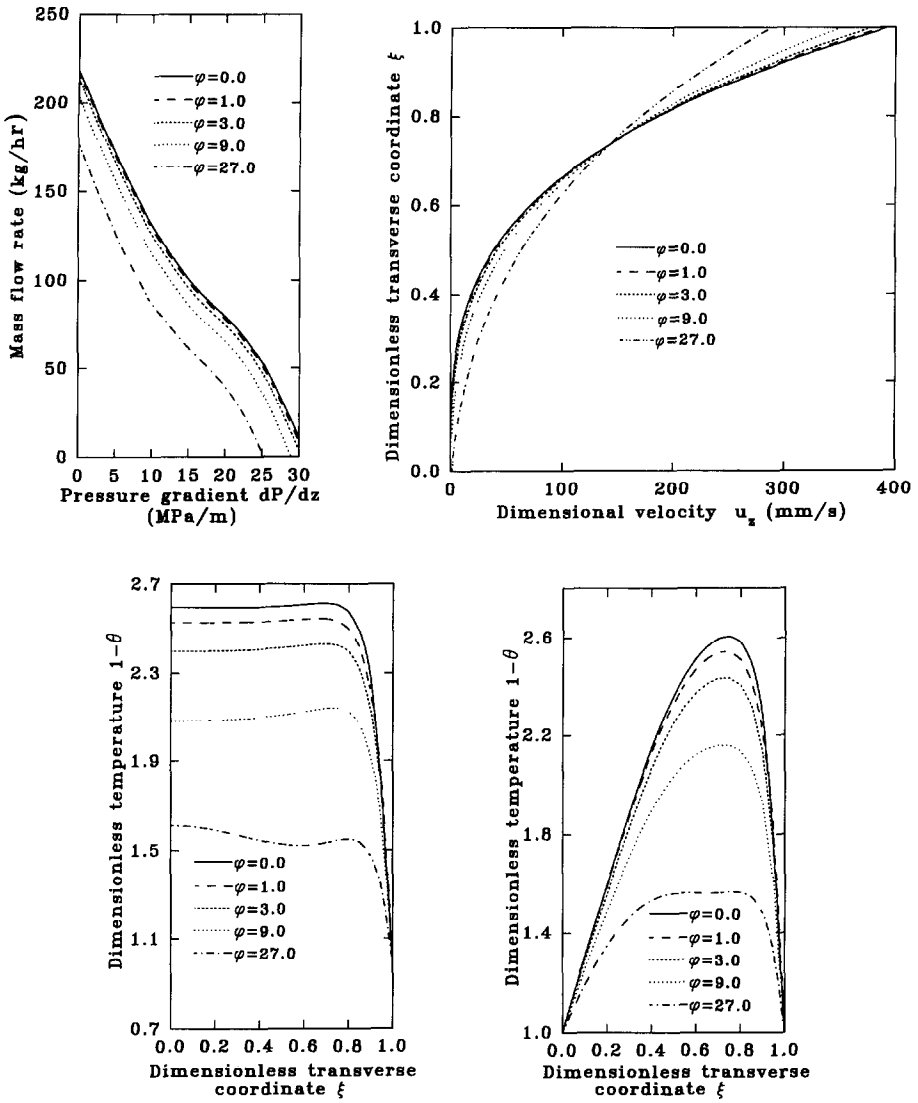

Fig. 7. (a) Mass flow rate vs pressure gradient relationship for an extruder for varying ratio of the slip coefficient at the barrel surface to the screw surface, φ; (b) dimensional transverse velocity profiles in an extruder channel for varying φ; (c) dimensionless transverse temperature profiles in an extruder channel with adiabatic screw root and isothermal barrel for varying φ; (d) dimensionless transverse temperature profiles in an extruder channel with isothermal screw and barrel for varying φ.

reverse behavior is obtained at the barrel surface. In the light of the velocity profiles, we can now examine the effect of the yield stress on the temperature profiles. For the adiabatic screw condition, at high values of τ_0, the dimensionless temperature rise increases from its value at the screw surface and, subsequently, decreases to the prescribed barrel temperature with the maximum fluid temperature occurring at a transverse location dependent on the value of τ_0. In addition, the temperature everywhere exceeds that of the barrel. In contrast, at lower values of τ_0, the dimensionless temperature rise monotonically decreases from the screw root value to that of the barrel.

At any transverse location, increased τ_0 gives rise to increased dimensionless temperature rise. In the screw region (Fig. 8(d)), even though one would expect the dimensionless temperature rise to decrease as τ_0 increases due to increased velocity and decreased velocity gradient, however, an opposite behavior is obtained. A closer examination of the viscous dissipation function $f(\xi)$ would provide the explanation for the opposite behavior. There are two driving forces for the viscous dissipation function $f(\xi)$, namely the velocity gradient and the yield stress both of which increase the viscous heating as they increase in value, but both of which are not independent as seen in Fig. 8(b–c). Therefore, even though the velocity gradient decreases as the yield stress increases, which would imply decreased temperature rise, the increase in yield stress appears to predominate for the chosen set of conditions, resulting in an increase in temperature rise.

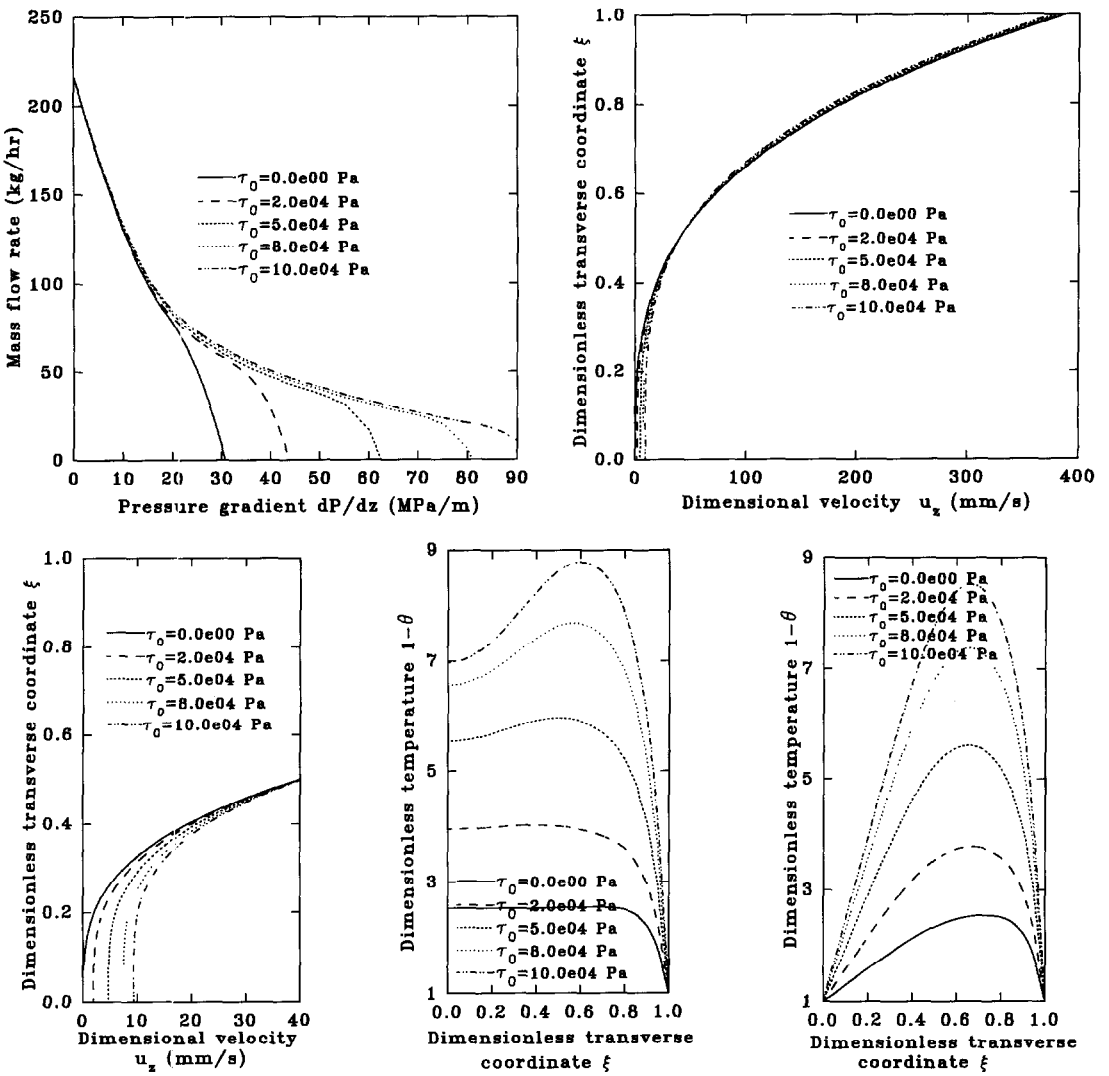

Fig. 8. (a) Mass flow rate vs pressure gradient relationship for an extruder for varying apparent yield stress τ_0; (b) dimensionless transverse velocity profiles in an extruder channel for varying apparent yield stress τ_0; (c) blown-up view of the dimensional transverse velocity profiles in the screw root region for varying apprarent yield stress τ_0; (d) dimensionless transverse temperature profiles in an extruder channel with adiabatic screw and isothermal barrel for varying apparent yield stress τ_0; (e) dimensionless transverse temperature profiles in an extruder channel with isothermal screw and barrel for varying apparent yield stress τ_0.

In the barrel region, the velocity gradient increases while the fluid's velocity decreases with increased yield stress, with both effects producing increased dimensionless temperature rise. Essentially, they augment the effect of yield stress on the temperature rise. As the yield stress increases, the shear viscosity of the viscoplastic fluid increases, the fluid becomes more solid like and the viscous heating increases. The increase in temperature rise can be up to a factor of nine or more for a viscoplastic fluid with a high yield stress value. For the isothermal screw and barrel surfaces, the effect of the yield stress on the temperature profiles is qualitatively the same, except that due to the constraint of prescribed wall temperature, the maximum temperature rise occurs within the fluid (Fig. 8(e)).

(*d*) *Effect of the Griffith number G.* The predominant mechanism responsible for temperature rise in extrusion of highly viscous viscoplastic fluids is viscous dissipation. A few observations can be made. For adiabatic screw and isothermal barrel, at low values of G, the dimensionless temperature increases from its screw root value which is less than the barrel temperature to a maximum value at a transverse location very close to the barrel where the velocity gradient is highest. Thereafter, the temperature reduces to the prescribed barrel temperature. The barrel essentially heats the fluid. As the value of G increases, the screw root temperature also increases and at a certain G value, a reverse behavior is obtained with the fluid now heating the barrel due to the significant viscous dissipation effect. For example, when

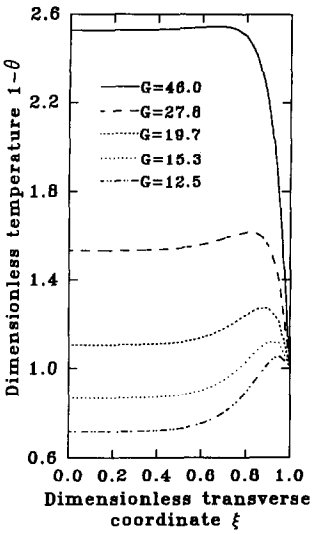

Fig. 9. Dimensionless transverse temperature profiles in an extruder channel with adiabatic screw and isothermal barrel for varying Griffith number G.

$G = 46.0$, the fluid temperature is everywhere higher than that of the barrel. At any transverse location within the fluid, increase in Griffith number increases the dimensionless temperature. The results are qualitatively similar for the isothermal screw and barrel surfaces thermal boundary condition and are, hence, not presented.

CONCLUSIONS

General analytical and exact solutions have been developed for a model of non-isothermal extrusion processing of viscoplastic fluids subject to wall slip. The model accommodates different slip coefficients at the screw and barrel surfaces. The solutions are applicable to the wide range of flow and heat transfer parameters encountered in extrusion processing operations, and comparisons between the model predictions and experimental data indicate that the solutions can be reliably used in the design of single screw and self-wiping intermeshing co-rotating twin screw extruders.

The solutions have been used in assessing the importance of such parameters as the slip coefficient β, the ratio of barrel surface slip coefficient to screw surface slip coefficient φ, the apparent yield stress τ_0 and the Griffith number G. The effect of both β and φ is a reduction of production rate for constant pressurization, while viscoplasticity produces an opposite effect. For the two thermal boundary conditions considered in this study, wall slip significantly moderates the temperature rise experienced by the processed material in the extruder, while increase in apparent yield stress increases the shear viscosity of the fluid thereby increasing the temperature rise. The Griffith number expectedly produces a significant effect on the temperature rise, with the temperature rise increasing with increased Griffith number.

Acknowledgement—A. Lawal would like to express his gratitude to KFUPM for making available the computing facilities required for the completion of the work. The experimental work summarized in this article was carried out by Ms B. Aral and Ms P. Yaras of HFMI. The typing of the manuscript was excellently done by Mr E. Esteban.

REFERENCES

1. Denson, C. D. and Hwang, B. K., The influence of the axial pressure gradient on flow rate for Newtonian liquids in a self-wiping, co-rotating twin-screw extruder. *Polymer Engineering Science*, 1980, **20**, 965–971.
2. Wang, Y. and White, J. L., Non-Newtonian flow modeling in the screw region of an intermeshing co-rotating twin-screw extruder. *Journal of Non-Newtonian Fluid Mechanics*, 1989, **32**, 19–38.
3. Kalyon, D. M., Gotsis, A. D., Yilmazer, U., Gogos, C., Sangani, H., Aral, B. and Tsenoglou, C., Development of experimental techniques and simulation methods to analyze mixing in co-rotating twin-screw extrusion. *Advances in Polymer Technology*, 1988, **8**, 337–353.
4. Lai-Fook, R. A., Senouci, A. and Smith, A. C., Pumping characteristics of self-wiping twin-screw extruders—a theoretical and experimental study on biopolymer extrusion. *Polymer Engineering Science*, 1989, **29**, 433–440.
5. Lawal, A. and Kalyon, D. M., Single screw extrusion of viscoplastic fluids subject to different slip coefficients at screw and barrel surfaces. *Polymer Engineering Science*, 1994, **34**, 1471–1479.
6. Fenner, T. R., Melt flow in polymer extrusion equipment. Ph.D. thesis, University of London, 1969.
7. Zamodits, H. J. and Pearson, J. R. A., Flow of polymer melts in extruders, Part 1: the effect of transverse flow and a superposed steady temperature profile. *Transactions of the Society of Rheology*, 1969, **13**, 357–385.
8. Colwell, R. E. and Nicholls, K. R., The screw extruder. *Industrial Engineering Chemistry*, 1959, **51**, 841–843.
9. Griffith, R. M., Fully developed flow in single screw extruders. *Industrial and Engineering Chemistry Fundamentals*, 1962, **1**, 180–187.
10. Ji, Z., Gotsis, A. D. and Kalyon, D. M., Single screw extrusion processing of highly filled suspensions including wall slip. *SPE ANTEC Technical Paper*, 1990, **36**, 160–163.
11. Jiang, T. Q., Young, A. C. and Metzner, A. B., The rheological characterization of hpg gels—measurement of slip velocities in capillary tubes. *Rheology Acta*, 1986, **25**, 397–404.
12. Kalyon, D. M., Yaras, P., Aral, B. and Yilmazer, U., Rheological behavior of a concentrated suspension: a solid rocket fuel simulant. *Journal of Rheology*, 1993, **37**, 35–53.
13. Boersma, W. H., Baets, P. J. M., Laven, J. and Stein, H. N., Time-dependent behavior and wall slip in concentrated shear-thickening dispersions. *Journal of Rheology*, 1991, **35**, 1093–1120.
14. Blyler, Jr, L. L. and Hart, Jr, A. C., Capillary flow instability of ethylene polymer melts. *Polymer Engineering Science*, 1970, **10**, 193–203.
15. Ramamurthy, A. V., Wall slip in viscous fluids and influence of materials of construction. *Journal of Rheology*, 1986, **30**, 337–357.
16. Atwood, B. T. and Schowalter, W. R., Measurements of slip at the wall during flow of high-density polyethylene through a rectangular conduit. *Rheology Acta*, 1989, **28**, 134–146.

17. Hatzikiriakos, S. G. and Dealy, J. M., Wall slip of molten high-density polyethylene—I. Sliding plate rheometer studies. *Journal of Rheology*, 1991, **35,** 497–523.
18. Chen, Y., Kaylon, D. M. and Bayramli, E., Effects of surface roughness and the chemical structure of materials of construction on wall slip behavior of linear low density polyethylene in capillary flow. *Journal of Applied Polymer Science*, 1993, **50,** 1169–1177.
19. Yilmazer, U. and Kalyon, D. M., Slip effects in capillary and parallel disk torsional flows of highly filled suspensions. *Journal of Rheology*, 1989, **33,** 1197–1212.
20. Mikhailov, M. D. and Ozisik, M. N., *Unified Analysis and Solutions of Heat and Mass Diffusion*. Wiley, New York 1984.
21. Cotta, R. M. and Ozisik, M. N., Laminar forced convection of power-law non-Newtonian fluids inside ducts. *Warme-und Stoffubertragung*, 1986, **20,** 211–218.
22. Mikhailov, M. D. and Vulchanov, N. L., Computational procedure for Sturm–Liouville problems. *Journal of Computational Physics*, 1983, **50,** 323–336.
23. Silliman, W. T. and Scriven, L. E., Separating flow near a static contact line: Slip at a wall and shape of a free surface. *Journal of Computational Physics*, 1980, **34,** 287–313.
24. Ybarra, R. M. and Eckert, R. E., Viscous heat generation in slit flow. *AIChE Journal*, 1980, **26,** 751–762.
25. Dinh, S. M. and Armstrong, R. C., Non-isothermal channel flow of non-Newtonian fluids with viscous heating. *AIChE Journal*, 1982, **28,** 294–301.
26. Esseghir, M. and Sernas, V., A cam-driven probe for measurement of the temperature distribution in an extruder channel. *SPE ANTEC Technical Paper*, 1991, **37,** 54–57.
27. Yaras, P., Rheological behavior and twin-screw extrusion flows of non-colloidal concentrated suspensions. Ph.D. thesis, Stevens Institute of Technology, Hoboken, NJ, 1995.
28. Aral, B., Flow and deformation behavior of concentrated suspensions; development of yield stress, viscoelasticity, wall slip and air entrainment effects. Ph.D. thesis, Stevens Institute of Technology, Hoboken, NJ, 1995.
29. Kalyon, D. M. and Gokturk, H., US Patent, 5 277 058, 1994.
30. Fenner, R. T., Extrusion (flow in screw extruders and dies). In *Computational Analysis of Polymer Processing*, eds J. R. A. Pearson and S. M. Richardson. Applied Science Publishers, New York, 1983, pp. 93–138.